Advances in Renewable Energies Offshore – Guedes Soares (Ed.)
© 2019 Taylor & Francis Group, London, ISBN 978-1-138-58535-5

A reduced wave-to-wire model for controller design and power assessment of wave energy converters

M. Penalba & J.V. Ringwood
Centre for Ocean Energy Research, Maynooth University, Maynooth, Co., Kildare, Ireland

ABSTRACT: Precise mathematical models are essential for designing energy maximising control strategies and assessing power production capabilities of Wave Energy Converters (WECs). However, commonly used mathematical models excessively simplify Wave-Structure Hydrodynamic Interactions (WSHIs) and/or the Power Take-Off (PTO) system, due to the need for fast models, resulting in poor control strategies and misestimated power production estimates. The suitability of a reduced Wave-to-Wire (rW2W) model is studied here, which includes only the necessary dynamics and losses of the WSHI and PTO system, significantly reducing mathematical requirements of a comprehensive High-Fidelity W2W (*HFW2W*) model. Results demonstrate that the controller designed using the *rW2W* model is very similar to that designed via the *HFW2W* model, ensuring a satisfactory performance of the WEC. In addition, power production capabilities of a WEC assessed using the *rW2W* and *HFW2W* models show very similar results, with differences of up to 5% in the annual mean power production.

1 INTRODUCTION

Precise mathematical models are crucial for the development of successful wave energy converters (WECs), to help developers and researchers better understand the behaviour of WECs. The energy generated from ocean waves passes through several conversion stages before it is converted into electricity and delivered into the electricity grid. Depending on the power take-off (PTO) system implemented in the WEC, the path from ocean waves to the electricity grid can be divided into between two and four conversion stages: *absorption*-, *transmission*-, *generation*- and *conditioning*-stage, as illustrated in Figure 1. Note that distinction between power absorption and generation is made intentionally, where absorption refers to the conversion of the energy stored in ocean waves into mechanical energy (motion of the absorber or the water column) and generation refers to the conversion of this mechanical energy into electricity.

Therefore, mathematical models that accurately represent each of these conversion stages are necessary. Figure 1 also shows that the different conversion stages are interconnected, meaning that any perturbation in one of the conversion stages may have an impact on the preceding and/or following conversion stage. As a consequence, not only separate mathematical models for each conversion stage are necessary, but also models that include all the essential subsystems and conversion stages from ocean waves to the electricity grid, known as wave-to-wire (W2W) models.

Wave-to-wire models that include different types of absorbers and PTO systems are suggested in the literature. Igic et al. (2011) present a W2W model for an overtopping device, including a low-head hydraulic turbine coupled to an electric generator. Similarly, W2W models for oscillating

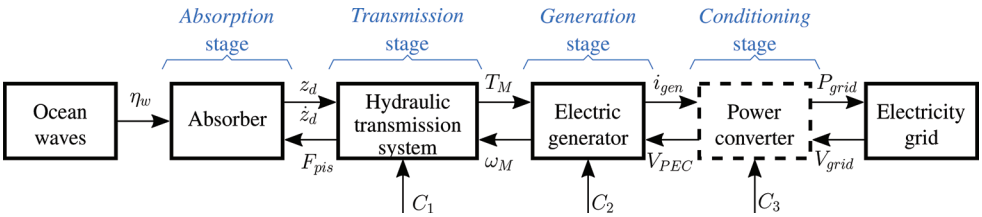

Figure 1. Diagram of a W2W model with a hydraulic PTO system, including all the subsystems and conversion stages from ocean waves to the electricity grid.

water column (OWC) devices, where air-turbines and electric generators are also incorporated, are suggested by Bailey et al. (2016) and Kelly et al. (2016). However, the vast majority of W2W models in the literature include wave-activated point absorbers (PAs) connected to different PTO systems: hydraulic PTO systems are suggested by Josset et al. (2007) and Hansen et al. (2011) for the SEAREV and Wavestar prototypes, respectively, a mechanical belt-drive PTO system is studied by Sjolte et al. (2013) for the Lifesaver converter, and Polinder et al. (2004) present a linear generator for the Archimedes Wave Swing prototype. Penalba and Ringwood (2016) provide more insight on W2W models with different PTO systems. Since the vast majority of WECs suggested in the literature include hydraulic PTO systems, a hydraulic PTO system is also considered in this study, as illustrated in Figure 1. More specifically, a variable-pressure hydraulic transmission system is used in this paper, due to it higher flexibility to actively control the behaviour of the absorber and maximise energy generation, as demonstrated by Penalba and Ringwood (2018a).

The remainder of the paper is as follows: Section 2 introduces the problem of using simplified mathematical models for controller design and power assessment, Section 3 presents the high-fidelity W2W model, Section 4 describes the reductions performed to create the reduced W2W model, Section 5 presents the selected location, WEC, PTO system and control strategies, Section 6 shows the results of control parameter optimization and power production assessment using the two mathematical models, and Section 7 draws the conclusions of the study.

2 CONTROLLER DESIGN AND POWER ASSESSMENT

Accurate power production assessment is vital for the development of successful WECs and wave energy projects. The predominant method for assessing power production capabilities is using the power matrix of the WEC, which is commonly calculated using mathematical models. This power matrix is then combined with the scatter diagram that characterises the resource of the specific location where the WEC is meant to be deployed. The approach with power matrices is employed recurrently in the literature for diverse purposes: Babarit et al. (2012) analyse power production capabilities of different WECs in different geographical locations, Penalba et al. (2017) study the effect of WEC array layouts in different wave climates, De Andres et al. (2016) assess the techno-economic feasibility of different WECs, and Ulazia et al. (2018) evaluate the impact of wave resource variations on WECs' power production.

However, potential inaccuracies of the power matrix approach can result in significant misestimation of the power production capabilities. Mérigaud and Ringwood (2018) discuss the suitability of the power matrix approach and suggest the use of full spectrum representation to minimise the misestimation of power production capabilities. However, the power matrix representation is used in the present paper, due to its simplicity and its appealing computational properties. Indeed, this paper focuses on the inaccuracies arisen due to an excessively simplified description of the WEC, rather than a poor characterisation of the resource.

Another important aspect when assessing power production capabilities, is the control strategy implemented in the WEC. Different control strategies have been suggested in the literature, demonstrating the benefits of actively controlling WECs. The need for precise mathematical models to design controllers that accurately maximise energy generation of WECs is shown by Penalba et al. (2017). However, mathematical models commonly used for the design of energy maximising control strategies and power assessment are excessively simplified models: wave-structure hydrodynamic interactions (WSHIs) are typically represented using the linear potential flow theory (using Cummins' equation (Cummins 1962) with viscous effects added externally via a Morsion-like equation (Morison et al. 1950)) and the PTO system is normally neglected. This simplified model is referred to as the *viscLPF+iPTO* model in the following.

With regard to the need for precise mathematical models for the design of controllers and power production assessment of WECs, Penalba and Ringwood (2018b) report the dramatic consequences of employing the *viscLPF+iPTO* model. Apart from the significant overestimation of the power production capabilities estimated with the *viscLPF+iPTO* model, controllers designed using the *viscLPF+iPTO* model force the WEC to follow a highly inaccurate trajectory that results in negative annual mean power production (AMPP) values, or, more dramatically, in situations where the device is permanently stuck at one of the end-stops of the PTO system.

Hence, Penalba and Ringwood (2018b) demonstrate the need for high-fidelity W2W mathematical models to accurately design the controller and assess power production capabilities. However, computational requirements of such a high-fidelity W2W model are prohibitive for applications where several cases need to be analysed, including the design of controllers or power production assessment.

In this respect, Penalba and Ringowood (2018) present a systematic model reduction approach

to design reduced W2W models that retain the application-relevant fidelity, while moving into a computationally feasible range. The high-fidelity simulation platform *HiFiWEC* presented in (Penalba et al. 2018), where a Computational Fluid Dynamic (CFD)-based numerical wave tank (NWT) is coupled to a high-fidelity power take-off model, is used as a basis for the complexity reduction. The reducedW2W model designed for power assessment and controller design, henceforth referred to as *rW2W* model, retains up to 95% fidelity compared to the *HiFiWEC* simulation platform, while reducing computational requirements to the level of the *viscLPF+iPTO* model.

Thus, the present paper studies the suitability of this *rW2W* model, comparing the results to the high-fidelity W2W (HFW2W) model used in (Penalba and Ringwood 2018b).

3 HIGH-FIDELITY WAVE-TO-WIRE MODEL

The *HFW2W* model is presented in (Penalba and Ringwood 2018a) and is validated using results measured in experimental test-rigs or generated with high-fidelity well-known software, and includes a computationally efficient multi-rate time-integration scheme.

3.1 *Wave structure hydrodynamic model*

The WSHI in the *HFW2W* model is represented using an extended version of Cummins' equation, including nonlinear FK forces (F_{FK}) and viscous effects (F_{visc}) as follows,

$$\begin{aligned}\left(\mathbf{M}+\mu_{\infty}\right)\ddot{x} = F_{FK} - F_{diff} - \int_0^t K_{rad}\left(t-\tau\right)\dot{x}\left(\tau\right)dt \\ + F_{visc} + F_{pis} + F_{EndStop}\end{aligned} \quad (1)$$

where M is the mass of the absorber, μ_{∞} the added mass at infinite frequency, x, $\dot{x}$ and $\ddot{x}$ the displacement, velocity and acceleration of the absorber, respectively, F_{diff} the diffraction force, K_{rad} the radiation impulse response function, F_{pis} the piston, and $F_{EndStop}$ the end-stop force. F_{FK} is solved algebraically calculating the pressure field over the instantaneous wetted surface using the computationally efficient method suggested by Giorgi and Ringwood (2017).

3.2 *Power take-off model*

The PTO system model includes all the important dynamics and losses of a hydraulic transmission system coupled to an electric generator. The hydraulic PTO system implemented in the *HFW2W* model includes a hydraulic cylinder, a low-pressure accumulator, relief-valves and a variable-displacement hydraulic motor. The mathematical model for the cylinder includes end-stop constraints, friction losses, and compressibility and inertia effects, providing the final piston force (F_{pis}) as follows,

$$F_{pis} = A_p \Delta p + F_{fric} + F_{in} \quad (2)$$

where A_p is the piston area, Δp the pressure difference between the cylinder chambers, F_{fric} the friction force modelled following the Stribeck formula (Jelali and Kroll 2012) and F_{in} the inertia force.

Pressure dynamics in cylinder chambers, including compressibility effects, are given as,

$$\dot{p} = \frac{\beta_{eff}}{V_{cyl} + A_p x_p}\left(Q - \dot{x}_p A_p\right) \quad (3)$$

where β_{eff} is the effective bulk modulus, V_{cyl} the minimum volume in the cylinder chamber, x_p and $\dot{x}_p$ are the piston position and velocity, respectively, and Q is the flow entering or exiting the cylinder chamber.

To maximise the energy generation of a WEC, an optimal control force (F^*_{PTO}) is generated in the controller. Two control strategies, *i.e.* resistive and reactive control, are implemented in this paper. Resistive and reactive control are implemented using control parameters B_{PTO} and K_{PTO} as in Equation (4), with $K_{PTO} = 0$ in the resistive control case. This F^*_{PTO} is then used to estimate the optimal pressure difference between the hydraulic cylinder chambers (Δp^*), which, in turn, is employed to define the fractional displacement of the hydraulic motor (α), the actual control input of the PTO system (C_1 in Figure 1).

$$F^*_{PTO} = -\left(xK_{PTO} + \dot{x}B_{PTO}\right) \rightarrow \Delta p^* = F^*_{PTO} / A_p \quad (4)$$

Hydraulic motors convert hydraulic pressure and flow into mechanical torque and rotational speed of the motor shaft coupled to an electric generator. The model of the hydraulic motor includes losses due to friction and leakages via the Schlösser loss model (Schlösser 1961). The output flow (Q_M) and torque of the motor (T_M) can be described as follows,

$$Q_M = \alpha D_{\omega} \omega_M - Q_{losses}, \quad (5)$$

$$T_M = \alpha D_{\omega} \Delta p_M - T_{losses} \quad (6)$$

where D_{ω} is the displacement of the hydraulic motor, ω_M the rotational speed of the shaft, Δp_M

the pressure difference across the hydraulic motor, and Q_{losses} and T_{losses} represent volumetric and mechanical losses in the hydraulic motor.

Finally, with respect to the electric generator, the model of a squirrel cage induction generator is implemented, following the equivalent two-phase *dq* equations presented in (Krause et al. 2013),

$$V_{sd} = R_s i_{sd} - \omega\lambda_{sq} + L_s \frac{d}{dt} i_{sd} + L_m \frac{d}{dt}\left(i_{sd} + i_{rd}\right), \quad (7)$$

$$V_{sq} = R_s i_{sq} + \omega\lambda_{sd} + L_s \frac{d}{dt} i_{sq} + L_m \frac{d}{dt}\left(i_{sq} + i_{rq}\right), \quad (8)$$

$$0 = R_r i_{rd} - \left(\omega - \omega_r\right)\lambda_{rq} + L_r \frac{d}{dt} i_{rd} + L_m \frac{d}{dt}\left(i_{sd} + i_{rd}\right), \quad (9)$$

$$0 = R_r i_{rq} + \left(\omega - \omega_r\right)\lambda_{rd} + L_r \frac{d}{dt} i_{rq} + L_m \frac{d}{dt}\left(i_{sq} + i_{rq}\right) \quad (10)$$

where V is the voltage, i the current, R the resistance and λ the flux. Subscripts s and r are used for the stator and rotor, while d and q refer to the direct and quadrature axes, respectively. ω and ω_r are the angular speed of the reference frame and the rotor, respectively.

The electromagnetic torque (T_e), rotational speed of the generator shaft and the generated electric power (P_e) are given by Equation (11),

$$T_e = \frac{3N_p}{4}\left(\lambda_{sd} i_{sq} - \lambda_{qs} i_{ds}\right), \quad (11)$$

$$\dot{\omega}_r = \frac{N_p}{2J_{shaft}}\left(T_e - T_M - B_{wind}\omega_r\right), \quad (12)$$

$$P_e = \frac{3}{2}\left(V_{sd} i_{sd} + V_{sq} i_{sq}\right) \quad (13)$$

where N_p is the number of poles in the generator, J_{shaft} the shaft moment of inertia and B_{wind} the friction/windage damping.

4 REDUCED WAVE-TO-WIRE MODEL

The WSHI model of the *rW2W* model is identical to that implemented in the *HFW2W* model. The complexity of the WSHI problem can be further reduced, but these reductions may lead to significant fidelity reductions. In contrast, the PTO system is significantly reduced in the *rW2W* model compared to the *HFW2W* model.

On the one hand, fluid compressibility is neglected in the hydraulic system, meaning that Δp in Equation (3) is the same as Δp^* in Equation (4).

On the other hand, the complexity of the electric generator is significantly reduced, neglecting electrical dynamics. Therefore, Equations (7)–(13), where all the required electrical dynamics of the rotor and stator are included, are replaced with their steady-state representations as follows,

$$T_e^{ss} = \frac{3\frac{Np}{2} R_r V_g^2}{s\omega_g\left[\left(R_s + R_r + \frac{1-s}{s} R_r\right)^2 + \omega_g\left(L_s + L_r\right)^2\right]} \quad (14)$$

$$P_e^{ss} = 3V_g I_e^{ss} cos\left(\angle Z^{ss}\right) \quad (15)$$

where V_g is the grid voltage, s the generator slip and ω_g the frequency of the grid voltage. The current at the stator is given as,

$$I_e^{ss} = \frac{V_g}{Z^{ss}}, \quad (16)$$

with

$$Z^{ss} = \frac{Z_r Z_m}{Z_r + Z_m} + Z_s. \quad (17)$$

Z_r, Z_s and Z_m are the rotor, stator and magnetizing impedances, respectively.

5 CASE STUDY

A case study is defined to compare the *HFW2W* and *rW2W* models, including the location, the absorber, and PTO and control characteristics.

5.1 *Absorber*

The selected WEC is a floating spherical buoy of 5-m diameter. However, for the sake of simplicity, the spherical buoy is restricted to heave motion only, as illustrated in Figure 2. Table 1 provides all the necessary information about the absorber.

5.2 *Location*

The WEC is analysed in Belmullet, off the west coast in Ireland, for which the Irish Marine Institute provided the data. Belmullet is one of the locations with the highest potential in Europe. The scatter diagram for Belmullet is shown in Figure 3, and the main characteristics of the location, such as the peak period and significant wave height with the highest frequency of occurrence (T_p' and H_s', respectively), and the mean annual incoming wave energy per meter of wave front (J) are presented in Table 1. Finally, it should be noted

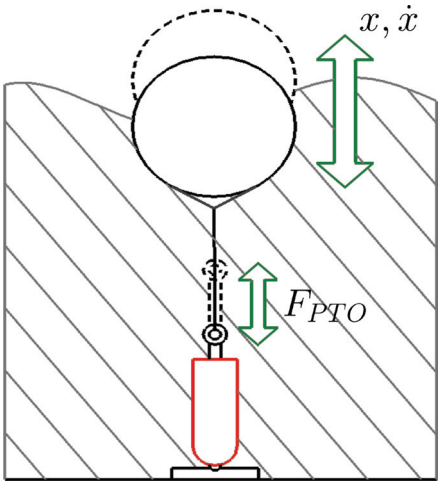

Figure 2. Diagram of the heaving PA WEC.

Table 1. Main characteristics of the selected location, the absorber and the PTO system.

Absorber	WEC diameter	5 m
	Mass	33.3 T
	Natural period	3.17 s
Location	T_p'	11.3 s
	H_s'	3.5 m
	J	78 kW/m
PTO	A_p	140 cm^2
	Cylinder length	2 m
	D_ω	1120 cc
	P_e^{rated}	74.5 kW
	J_{shaft}	4.45 kg·m^2

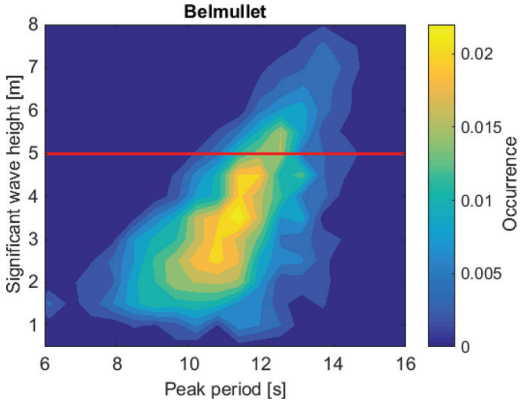

Figure 3. Scatter diagram of the Belmullet test site, where the red line shows the limit of WEC's operational space.

that the operational space of the WEC is limited to $H_s \leq 5m$, as illustrated by the red line in Figure 3.

5.3 *Power take-off design and control strategies*

The design of the PTO system is the same as that used in (Penalba and Ringwood 2018b). Table 1 presents the main characteristics of the PTO system implemented in the present paper. It should be noted that PTO components are not optimised and, therefore, results obtained with both mathematical models could probably be improved.

In addition to PTO system characteristics, the selection of an appropriate control strategy is crucial. In order to assess the suitability of the $rW2W$ model under different control conditions, both resistive and reactive control are analysed following Equation (4). The B_{PTO} and K_{PTO} parameters are optimised for each sea-state and mathematical model to maximize the energy generation. The optimisation is carried out via the exhaustive search algorithm, ensuring that the optimal value is always the global maximum.

6 RESULTS

Results are divided into two parts, where optimal control parameters and power production capabilities are compared in Sections 6.1 and 6.2, respectively. Both sections include a comparison between the $HFW2W$ and $rW2W$ models under resistive and reactive control, and differences are calculated in percentage terms as follows,

$$\Delta[\%] = \frac{y_{HFW2W} - y_{rW2W}}{y_{HFW2W}} \times 100 \tag{18}$$

where y_{HFW2W} and y_{rW2W} are the outputs from the $HFW2W$ and $rW2W$ models, respectively. Note that Δ can take positive or negative values, negative values meaning that outputs from the $rW2W$ model are overestimated, compared to the $HFW2W$ model.

6.1 *Control parameter optimisation*

Table 2 presents the optimal control parameters identified with the $rW2W$ and $HFW2W$ models. In addition, the impact of control parameters optimised with the $rW2W$ model are evaluated, using these control parameters to assess power production capabilities with the $HFW2W$ model, and comparing these power production estimates to the estimates obtained with control parameters optimised with the $HFW2W$ model. The differences between power production estimates (ΔP_e) are calculated following Equation (18). Preliminary

Table 2. Optimal control parameters and differences in power production estimations for the LE, ME and HE sea-states, using resistive and reactive control. Units of B_{PTO} and K_{PTO} are *kNs/m* and *kN/m*, respectively.

Resistive control	*rW2W*	*HFW2W*	
	B_{PTO}	B_{PTO}	ΔP_e [%]
LE	150	140	0.03
ME	210	210	0
HE	330	330	0
Reactive control	B_{PTO}/K_{PTO}	B_{PTO}/K_{PTO}	ΔP_e [%]
LE	70/70	–110/–120	5.2
ME	90/90	–160/–140	2.6
HE	150/160	–120/–140	3.2

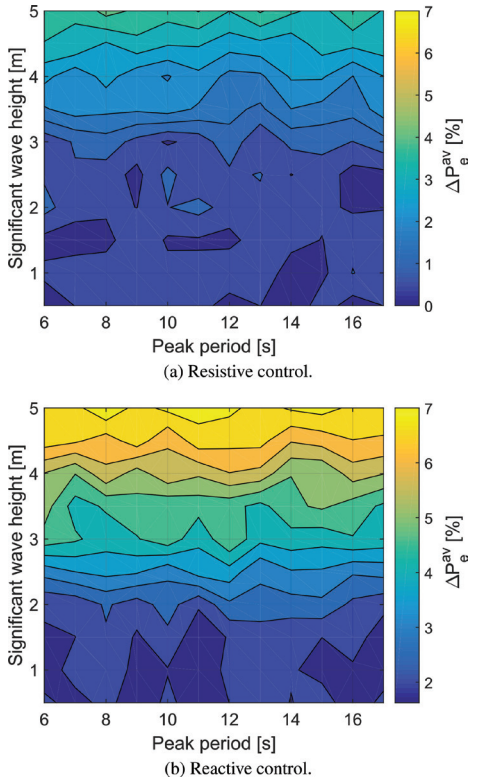

Figure 4. ΔP_e for the whole operational space under resistive (a) and reactive control (b).

results are presented for three sea-states in Table 2: a low-energetic (LE) sea-state ($T_p = 6s$ & $H_s = 1m$), a medium-energetic (ME) sea-state ($T_p = 8s$ & $H_s = 1.5m$) and a high-energetic (HE) sea-state ($T_p = 11s$ & $H_s = 3m$). These results are then extended to the whole operational space in Figure 4.

In the case of resistive control, control parameters optimised utilising the *rW2W* model are identical to those optimised with the *HFW2W* model, except for the LE sea-state, where B_{PTO} optimised with the *rW2W* model is slightly overestimated. In the reactive control case, differences are slightly larger, especially for the K_{PTO} term, with overestimation of up to 15%.

However, overestimation of control parameters has a very low impact on the power production estimates. Power generation differences ΔP_e are negligible under resistive control. Under reactive control, these differences increase, but remain reasonably low, up to 5%, where the highest differences are found for the LE sea-state. Note that all ΔP_e values in Table 2 are positive values, meaning that the *rW2W* model underestimates power production capabilities.

Figure 4(a) and (b) show the ΔP_e for all the different sea-states in the operational space under resistive and reactive control, respectively.

ΔP_e values are relatively low across the whole operational space for both control strategies. The *rW2W* model always underestimates power production, being this underestimation highest at HE sea-states, up to 4% and 7% under resistive and reactive control, respectively. However, differences under resistive control remain remarkably low, below 1%, for LE and ME sea-states, and only increase for HE sea-states ($H_s \geq 3m$).

A similar trend can be observed under reactive control, where ΔP_e values increase with H_s. However, differences at LE and ME sea-states are higher under reactive control, compared to the resistive control case. Results shown in Figure 4 are consistent with the results presented by Penalba and Ringwood (2018), where the ME sea-state is used, observing practically identical results for the *rW2W* and *HFW2W* models under resistive control, and a difference of about 2% under reactive control.

6.2 *Power assessment*

Power production capabilities of the spheric HPA are studied over the whole operational space shown in Figure 3, utilising the AMPP measure. Table 3 illustrates AMPP values of the spheric HPA at Belmullet. In addition to the AMPP values, PTO efficiency values (η_{PTO}) for the two mathematical models are shown in Table 3. PTO efficiency η_{PTO} is calculated using generated ($AMPP_{gen}$) and absorber AMPP values (AMPP*abs*), as follows:

$$\eta_{PTO} = \frac{AMPP_{gen}}{AMPP_{abs}} \cdot 100. \tag{19}$$

The absorption stage in both mathematical models is identical and, therefore, the η_{PTO} illustrates the differences between the *rW2W* and *HFW2W*

Table 3. Power production assessment of the spherical WEC under resistive and reactive control, including AMPP and PTO efficiencies obtained using the *rW2W* and *HFW2W* models; and $AMPP_{gen}$ values with misestimated control parameters. *AMPP* values are given in kW, while efficiencies are shown in percentage.

		rW2W	*HFW2W*	Δ [%]
Resistive control	$AMPP_{gen}$	19.16	19.89	3.7
	η_{PTO}	67.8	70.3	N/A[1]
	$AMPP_{gen}^{rW2W}$	N/A	19.72	0.8
Reactive control	$AMPP_{gen}$	34.32	36.17	5.1
	η_{PTO}	56.05	59.07	N/A
	$AMPP_{gen}^{rW2W}$	N/A	35.48	2.6

[1]The abbreviation N/A is used for *not applicable*.

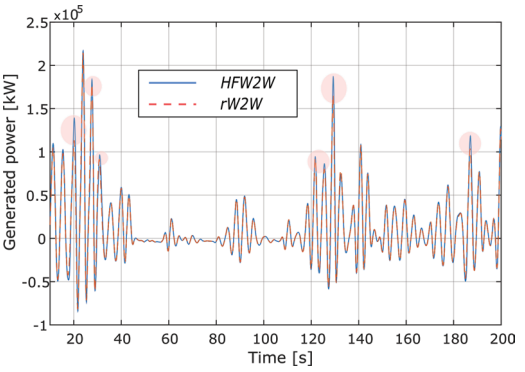

Figure 5. Generated power estimated with the *HFW2W* and *rW2W* models for the ME sea-state under reactive control.

models. Finally, Table 3 also shows AMPP values calculated via the *HFW2W* model, but using control parameters optimised with the *rW2W* model ($AMPP_{gen}^{rW2W}$). In the latter case, the difference Δ shown in Table 3 is given by the difference between $AMPP_{gen}^{rW2W}$ and $AMPP_{gen}$ calculated with the *HFW2W* model.

Differences between the *rW2W* and *HFW2W* models for the AMPP are remarkably low, where the *rW2W* underestimates power production capabilities of the spheric HPA by 3.7% and 5.1% under resistive and reactive control, respectively. Due to the high occurrence of the HE sea-states in Belmullet, differences between the two mathematical models are close to the differences at HE sea-states shown in Figure 4. On the other hand, the impact of control parameters optimised using the *rW2W* model on the performance of the WEC is demonstrated to be negligible under resistive control, a difference of 0.8%, and very low under reactive control, 2.6%.

The differences between the *rW2W* and *HFW2W* models appear due to the lower efficiency of the PTO system in the *rW2W* model, as shown in Table 3. However, the opposite is to be expected, since the trW2W model includes less dynamics than the *HFW2W* model, which suggests that losses should be higher in the *HFW2W* model. Figure 5 illustrates the generated power signal of the *HFW2W* and *rW2W* models for the ME sea-state under reactive control, where one can notice the underestimation of the *rW2W* model at some power peaks, highlighted with red circles. However, further investigation is required to find the reason why the *rW2W* model underestimates power capabilities.

In any case, differences between the *rW2W* and the *HFW2W* model are relatively low, providing optimal control parameters and reasonably high-fidelity power capability estimates. In addition, computational requirements of the *rW2W* model, reducing computational time in an order of magnitude, make the *rW2W* model the most suitable candidate for controller design and power assessment purposes, as suggested by Penalba and Ringwood (2018).

7 CONCLUSIONS

The present paper compares a comprehensive high-fidelity wave-to-wire model (*HFW2W*), where all the important components of the different conversion stages from ocean waves to the electricity grid are incorporated, to a reduced wave-to-wire model (*rW2W*), where only the most relevant dynamics are included, for the optimisation of control parameters and power production assessment.

Results from these two mathematical models are obtained for resistive and reactive control. Hence, control parameters and power production estimates provided by the *rW2W* model show good agreement, under both control strategies, with the results obtained using the *HFW2W* model. Differences are particularly low for resistive control, where control parameters optimised using both mathematical models are almost identical and differences in power production estimates are remarkably low, particularly at low- and medium-energetic sea-states. Although differences increase under reactive control, they still remain reasonably low.

Hence, given the reasonably high-fidelity results provided by the *rW2W* model and its appealing computational requirements, reducing by an order of magnitude the simulation time, the *rW2W* model is shown to be the ideal candidate to optimise control parameters (design controllers) and assess power production capabilities of WECs.

ACKNOWLEDGMENTS

This material is based upon works supported by Science Foundation Ireland under Grant No. 13/IA/1886.

REFERENCES

Babarit, A., J. Hals, M. Muliawan, A. Kurniawan, T. Moan, & J. Krokstad (2012). Numerical benchmarking study of a selection of wave energy converters. *Renewable Energy 41*, 44–63.

Bailey, H., B.R. Robertson, & B.J. Buckham (2016). Wave-to-wire simulation of a floating oscillating water column wave energy converter. *Ocean Engineering 125*, 248–260.

Cummins, W. (1962). The impulse response function and ship motion. *Schiffstechnik* (9), 101–109.

De Andres, A., J. Maillet, J. Hals Todalshaug, P. Möller, D. Bould, & H. Jeffrey (2016). Techno-economic related metrics for a wave energy converters feasibility assessment. *Sustainability 8*(11), 1109.

Giorgi, G. & J.V. Ringwood (2017). Computationally efficient nonlinear froude–krylov force calculations for heaving axisymmetric wave energy point absorbers. *Journal of Ocean Engineering and Marine Energy 3*(1), 21–33.

Hansen, R.H., T.O. Andersen, & H.C. Pedersen (2011). Model Based Design of Efficient Power Take-Off Systems for Wave Energy Converters. *Proceedings of the 12th Scandinavian International Conference on Fluid Power*, 1–15.

Igic, P., Z. Zhou,W. Knapp, J. MacEnri, H.C. Sorensen, & E. Friis-Madsen (2011, January). Multi-megawatt offshore wave energy converters – electrical system configuration and generator control strategy. *Renewable Power Generation, IET 5*(1), 10–17.

Jelali, M. & A. Kroll (2012). *Hydraulic servo-systems: modelling, identification and control*. Springer Science & Business Media.

Josset, C., A. Babarit, & A.H. Clément (2007). A wavetowire model of the searev wave energy converter. *Proceedings of the Institution of Mechanical Engineers, Part M: Journal of Engineering for the Maritime Environment 221*(2), 81–93.

Kelly, J.F., W.M.D. Wright, W. Sheng, & K. OSullivan (2016, April). Implementation and verification of a wave-to-wire model of an oscillating water column with impulse turbine. *IEEE Transactions on Sustainable Energy 7*(2), 546–553.

Krause, P.C., O. Wasynczuk, S.D. Sudhoff, & S. Pekarek (2013). *Analysis of Electric Machinery and Drive Systems* (3rd Edition ed.). IEEE Press Series on Power Engineering. Wiley-Blackwell.

Mérigaud, A. & J.V. Ringwood (2018). Power production assessment for wave energy converters: Overcoming the perils of the power matrix. *Proceedings of the Institution of Mechanical Engineers, Part M: Journal of Engineering for the Maritime Environment 232*(1), 50–70.

Morison, J.R., M., Johnson, J.W., Schaaf, & S.A. (1950). The Force Exerted by Surface Waves on Piles. *Journal of Petroleum Technology 2*(5), 149–154.

Penalba, M., J. Davidson, C. Windt, & J. Ringwood (2018). A high-fidelity wave-to-wire simulation platform for wave energy converters: Coupled numerical wave tank and power take-off models. *Applied Energy 226C*, 655–669.

Penalba, M., A. Mérigaud, J.-C. Gilloteaux, & J.V. Ringwood (2017). Influence of nonlinear froude–krylov forces on the performance of two wave energy points absorbers. *Journal of Ocean Engineering and Marine Energy 3*(3), 209–220.

Penalba, M. & J.V. Ringowood (2018). Systematic model complexity reduction of wave-to-wire models for wave energy system design. *Submitted to Applied Mathematic Modelling*.

Penalba, M. & J. Ringwood (2018a). A high-fidelity waveto- wire model for wave energy converters. *Submitted to Renewable Energy*.

Penalba, M. & J. Ringwood (2018b). The impact of wave-to-wire models in control parameter optimization and power assessment. In *Proceedings of the ASME 37th International Conference on Ocean, Offshore and Arctic Engineering, Madrid, Spain*, Number OMAE2018–77501.

Penalba, M. & J.V. Ringwood (2016). A review of wave-to-wire models for wave energy converters. *Energies 9*(7), 506.

Penalba, M., I. Touzón, J. Lopez-Mendia, & V. Nava (2017, July). A numerical study on the hydrodynamic impact of device slenderness and array size in wave energy farms in realistic wave climates. *Ocean Engineering 142*, 224–232.

Polinder, H., M.E. Damen, & F. Gardner (2004). Linear PM generator system for wave energy conversion in the AWS. *IEEE Transactions on Energy Conversionr 19*(3), 583–589.

Schlösser, W. (1961). Mathematical model for displacement pumps and motors. *Hydraulic power transmission*, 252–257.

Sjolte, J., C.M. Sandvik, E. Tedeschi, & M. Molinas (2013). Exploring the potential for increased production from the wave energy converter lifesaver by reactive control. *Energies 6*(8), 3706–3733.

Ulazia, A., M. Penalba, G. Ibarra-Berastegui, J. Ringwood, & J. Sáenz (2018). Wave energy trends over the bay of biscay and the consequences for wave energy converters. *Energy 141*, 624–634.